Variations of Midlatitude Transient Dynamics Associated with ENSO

DAVID M. STRAUS AND J. SHUKLA

Center for Ocean–Land–Atmosphere Studies, Calverton, Maryland

(Manuscript received 6 October 1995, in final form 1 March 1996)

ABSTRACT

The winter response of the atmosphere to El Niño events in the Pacific is studied both from a 14-year integration of the Center for Ocean–Land–Atmosphere GCM using observed SSTs from January 1979 to February 1993 and from the corresponding analyses of ECMWF. Emphasis is put on the shift in the high-frequency transients that define the Pacific storm track during warm events. Warm and normal ensembles are defined on the basis of the GCM's diabatic heating field in the tropical Pacific, which falls in one of two states. During the winters of 1982/83, 1986/87, and 1991/92, the heating averaged between 6°S and 6°N lies in the range of 100–200 W m^{-2} all the way across the basin. The remaining 10 ''normal'' years all show no large tropical diabatic heating anomalies in the mid or eastern Pacific.

The difference between warm and normal ensembles for the mean fields of zonal wind u and height z indicates an eastward and equatorward extension of the midlatitude Pacific jet, associated with a similar extension of the transient feedback on the mean flow as measured by the convergence of vorticity flux. The increase in high-frequency (periods of ~2 to 10 days) transient kinetic energy in the eastern portion of the Pacific during El Niño extends across Mexico. The high-frequency transient vertical and meridional sensible heat fluxes, and the low-level diabatic heating and baroclinicity of the mean state (measured by $Ri^{-1/2}$) also indicate an eastward and equatorward shift of the entire storm track complex in the GCM and the analyses. The shift is consistent with the increased midlatitude shear during El Niño that accompanies the overall tropical warming.

While the GCM storm track shift has strong similarities to that in the analyses, the GCM's large systematic errors in the mid Pacific (eastward extension of the Pacific jet and the storm track) lead to an underestimation of the response to El Niño, which has a very similar form. However, the GCM also shows a spurious tendency to move the storm tracks equatorward in the far western Pacific, as seen in the large positive anomalies in all dynamical indicators of the storm tracks at latitudes 20°–30°N.

1. Introduction

The influence of the extensive warm anomalies of sea surface temperature (SST) in the central and eastern tropical Pacific associated with the El Niño–Southern Oscillation phenomenon on the winter circulation in northern midlatitudes has been a subject of intense study during the past decade. Not only do these SST anomalies represent a particularly potent example of the type of boundary forcing that forms the physical basis of potential atmospheric predictability on the seasonal time scale (Shukla 1984, 1985), but the strong links to the winter climate in the Pacific–North America (PNA) region (Bjerknes 1966,1969; Horel and Wallace 1981; van Loon and Madden 1981) have practical implications for seasonal forecasting over North America (Livezey and Mo 1987). While the midlatitude stationary wave anomalies associated with the warm SSTs have received a great deal of attention both from the theoretical point of view (Hoskins and Karoly 1981; Sardeshmukh and Hoskins 1988) and the modeling perspective (Shukla and Wallace 1983; Blackmon et al. 1983; Fennessy et al. 1985; Lau 1985; Palmer and Mansfield 1986; Fennessy and Shukla 1988; Lau and Nath 1994; Smith 1995), considerably less attention has been paid to the characteristics of the transient anomalies. The analysis of results of general circulation models that utilized linearized versions of the models forced by tropical diabatic heating and transient fluxes has elucidated the important role played by the transient vorticity fluxes in extending the Pacific wintertime jet and the associated regions of high synoptic variability at upper levels downstream (eastward) into the far eastern Pacific (Kok and Opsteegh 1985; Ting and Held 1990; Hoerling and Ting 1994; Peng 1995). Analogous results obtained from archives of operational analyses have been reported in papers by Hoerling and Ting (1994) and Rasmusson and Mo (1993). Since the focus of all these studies is on the far eastern edge of the Pacific storm track, the emphasis on barotropic dynamics is consistent with earlier work on storm track dynamics (Simmons and Hoskins 1978).

Yet the broader issue of the response of the entire

Corresponding author address: Dr. David M. Straus, Center for Ocean–Land–Atmosphere Studies, 4041 Powder Mill Road, Suite 302, Calverton, MD 20705.
E-mail: straus@cola.iges.org

Pacific baroclinic storm track to the shift in tropical heating accompanying warm events, and in particular the response of eddies in regions further west (and closer to the coast of Asia) marked by rapid development and the dominance of baroclinic dynamics, has been touched upon only by Trenberth and Hurrell (1994), who show that the observed storm tracks shift equatorward during warm events. Are the changes seen in the eastern Pacific during warm events (which we refer to as El Niños), in which the extension of the jet enables individual storms to penetrate into North America (Schonher and Nicholson 1989; Cavazos and Hastenrath 1990), part of a more systematic change in storm track dynamics?

The purpose of this paper is to study this question, using both the operational analyses of the European Centre for Medium-Range Weather Forecasts (ECMWF) for the period 1980–1993 and a 14-year integration of the high resolution Center for Ocean–Land–Atmosphere (COLA) GCM, forced by observed SSTs for the period 1979–1993. Use of the GCM simulation has the double advantage of consistency over time and access to the diabatic heating field (which is not available from analyses). Clearly the GCM also has errors, and the systematic error in particular can impact the simulation of El Niño-related changes quite severely (Hoerling and Ting 1994; Peng 1995). Thus, we interpret the comparison between the diagnosis of the GCM and ECMWF storm tracks primarily as a verification of the model, but also as an approach to further understand the results from the analyses.

Any attempt to define a midlatitude response in (either stationary or transient) flow to tropical SST anomalies must recognize the inherently chaotic nature of the midlatitude circulation. Since the degree of ''natural variability'' (i.e., variability unrelated to boundary condition changes) is so large in midlatitudes, one can expect at most that the influence of SST anomalies (whether tropical or not) will be to modify the probability density function of the midlatitude circulation in some manner (Palmer 1993; Kumar and Hoerling 1995). Thus the problem of relating midlatitude circulation changes to SST anomalies becomes essentially a stochastic one (see recent summaries in Barnett 1995 and Stern and Miyakoda 1995). Extracting the SST-related ''signal'' from the ''noise'' generated by midlatitude internal dynamics requires ensemble averaging. These comments apply equally well to the observed atmospheric variations and those modeled by the GCM (Barnett 1995), although there is a tendency in the literature to ignore the stochastic nature of the ''real'' as opposed to the model climate.

In this paper we define an ensemble of winters corresponding to warm events, and an ensemble of ''normal'' winters. The definitions of these ensembles are based not on the tropical SST anomalies directly, but on the GCM's tropical *diabatic heating* anomalies that are generated in response to the SST anomalies. This approach is physically consistent with the conceptual

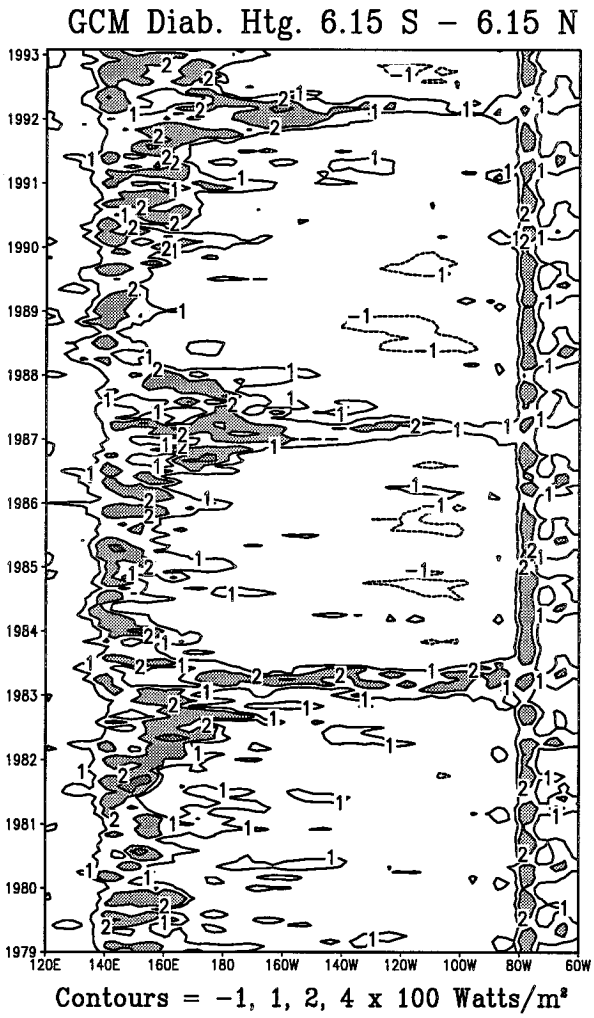

FIG. 1. Vertically integrated diabatic heating, averaged between 6.15°S and 6.15°N, plotted from monthly mean data from 120°E to 60°W. Units are 100 W m^{-2}. Contours at −1, 1, 2, 4. Shaded values are greater than 2.

model of the deep tropical diabatic heating anomalies as the critical link between El Niño SST anomalies and the midlatitude dynamical response. Based on the evolution of the GCM's tropical diabatic heating (to be shown in Fig. 1), we define the warm ensemble as the winters of 1982/83, 1986/87, and 1991/92. The normal or ''nonwarm'' ensemble is defined as the 10 other winters from 1980/81 to 1992/93 (i.e., all winters excluding the warm winters). Since the GCM's tropical diabatic heating anomaly during the ''cold'' event of 1988/89 is weak, this event is considered to be part of the normal ensemble. We average each diagnostic over the two ensembles separately. The differences between these averaged statistics can then be assessed with a standard *t* test. This procedure enables us to treat both the ECMWF analyses and the COLA GCM results on a completely equal footing.

The plan of the paper is as follows. The GCM and

the extended integration as well as the analyzed ECMWF data are described in section 2. The evolution of the tropical diabatic heating in the GCM, which motivates the definitions of the ''warm'' and normal ensembles, is discussed in section 3. Section 4 discusses warm minus normal winter mean state differences in both the GCM and the ECMWF analyses, and presents a measure of a spatially dependent pattern correlation between the two. The influence of the GCM's systematic error is also brought out. Transient statistics that elucidate the various dynamical regimes of the storm tracks are presented in section 5, and the summary and discussion are given in section 6.

2. GCM and analysis data

The COLA GCM uses moderately high-resolution spectral dynamics (rhomboidal 40) with 18 discrete levels in the vertical. Precipitation is controlled by specific humidity criteria as well as by parameterizations of cumulus and shallow convection. Cloud–radiation interaction and gravity wave drag schemes are included. A second-order turbulence closure scheme takes into account the effects of vertical diffusion, and the simplified SiB (Xue et al. 1991) determines the effects of vegetation on the transfer of momentum, latent heat, and sensible heat at the biosphere–atmosphere interface. Soil moisture is predicted in three layers. Further details of the COLA GCM can be found in Kinter et al. (1988) and Xue et al. (1991) and references therein.

The extended integration of the COLA GCM was initialized with data valid for 0000 UTC 1 January 1979 (obtained from the National Centers for Environmental Prediction, formerly the the National Meteorological Center) and was integrated through the end of February 1993 (170 months) utilizing observed monthly mean SSTs and sea-ice extent (Reynolds 1988; Gates 1992). The first 10 years of the integration (1979–1988) were carried out in cooperation with the Atmospheric Model Intercomparison Project, which has been supported by the Working Group on Numerical Experimentation of the World Climate Research Programme (Gates 1992).

The GCM data used in this study were all sampled once per day, and were interpolated to the seven pressure levels: 1000, 850, 700, 500, 300, 200, and 100 hPa. The only exception was the total diabatic heating (and rainfall), which was averaged (accumulated) over all time steps in each day and written out once per day. In addition, the diabatic heating shown in Fig. 1 below was vertically integrated using the original GCM vertical coordinate.

The analyses of the ECMWF were obtained at a twice-daily frequency from the National Center for Atmospheric Research. For documentation on this dataset, see for example Trenberth and Olson (1988).

This paper concentrates on the winter season, which was defined as the 128-day period starting from the 11th of November of each year. The 13 winters that are common to the GCM and the analyses (1980/81 through 1992/93) were used in the calculations presented here.

The seasonal mean in this paper is simply the 128-day mean. However, the transient component is defined as the deviation from the annual cycle component. For each winter season, an estimate of the annual cycle component was obtained by projecting the time series for each variable at each grid point onto the first three Legendre polynomials in time, following Straus (1983). This method is equivalent to using the best-fit parabola (in time). By using the estimate of the annual cycle component for each winter separately, the interannual changes in the seasonal mean do not contribute at all to the transients. (This would not be the case if the transients were defined as the deviations from the ensemble mean of all the winter parabolas.)

3. Tropical heating anomalies

The eastward migration of warm SSTs in the tropical Pacific during El Niño is accompanied by a similar migration of rainfall (Quiroz 1983) and hence total diabatic heating. Figure 1 presents the entire history of monthly mean vertically integrated GCM diabatic heating as a function of longitude and month, averaged over the latitudes 6.15°S–6.15°N. The heating is given as a change in enthalpy in units of watts per square meter and is calculated directly from the model's original (sigma) vertical levels. The three warm events are seen as striking extensions of the western Pacific maximum all the way across the ocean basin during the winters of 1982/83, 1986/87, and 1991/92. The corresponding plot of GCM precipitation (not shown) is very similar to Fig. 1 and agrees well with the results obtained from the satellite estimates of observed precipitation from microwave sounding unit (MSU) data (Spencer 1993) with regard to the extent of the El Niño anomalies. However, the simulated excursions of precipitation into the eastern Pacific occur later in the El Niño winters than is observed, typically by one month.

The primary mode of variation of the entire tropical model heating is thus seen to be closely related to El Niño. While differences between the heating patterns during the three events are seen in Fig. 1 and in maps of the individual heating anomalies (not shown), they are far more similar to each other than to the climatological pattern, motivating the consideration of these events as an ensemble. The difference in precipitation for the warm ensemble average (three winters) and the normal ensemble average (10 winters) is shown for the MSU data in Fig. 2a and for the GCM in Fig. 2b. The shaded area indicates significance at the 95% level using a standard *t*-test (see appendix for details). While the pattern of positive anomaly straddling the equator shows good agreement, the compensating negative (drying) anomalies seen in the central and western Pacific are shifted north in the GCM results. The vertical structure of the warm ensemble heating anomaly compared to the

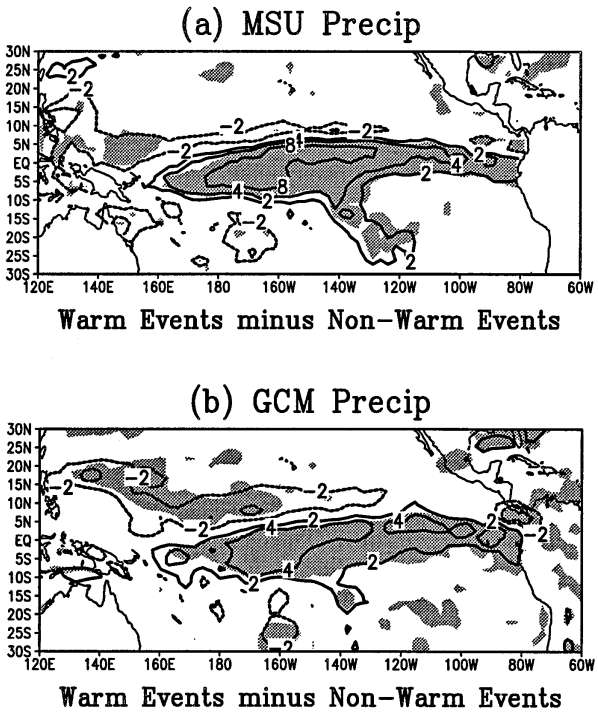

FIG. 2. Difference of seasonal mean precipitation between warm and normal ensembles. (a) Satellite (MSU) derived values. (b) COLA GCM values. Units are mm/day, with contours at −8, −4, −2, 2, 4, and 8. Shading indicates significance at the 95% level.

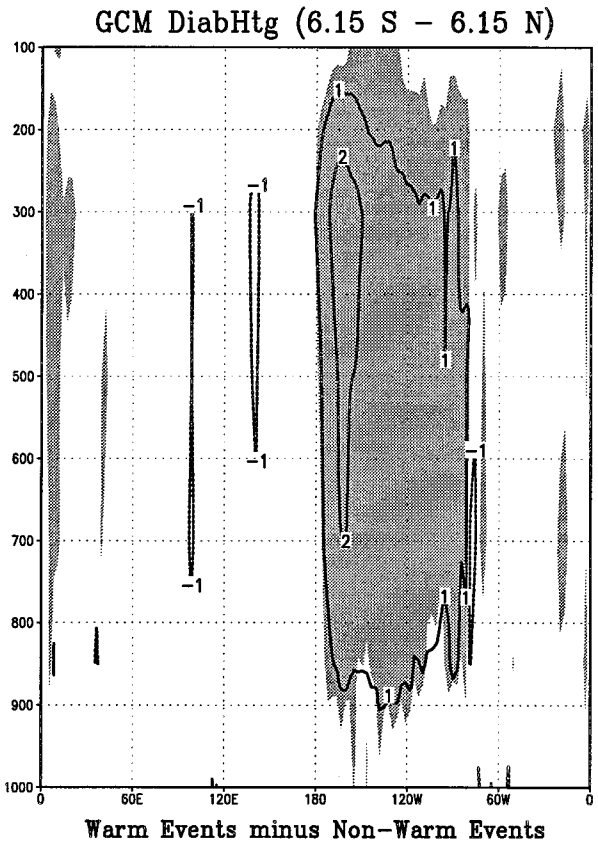

FIG. 3. Pressure–longitude plot of the seasonal mean diabatic heating difference from the GCM between warm and normal ensembles, averaged from 6.15°S to 6.15°N. Shading indicates significance at the 95% level. Units are degrees per day.

normal ensemble is seen in Fig. 3 for the latitude band 6.15°S–6.15°N. (Here the calculation was done on pressure surfaces and is reported as a change in temperature in degrees/day.) A deep structure with maximum anomaly of 2 K/day east of the date line at 300 hPa is seen. The shaded area indicates significance at the 95% level.

4. Winter seasonal mean differences

In order to quantify the agreement between the simulated seasonal mean fields and those in the ECMWF analyses, particularly with respect to the occurrence of El Niño, we introduce a quantity termed the ''correlation field.'' This quantity is a generalization of the spatial anomaly correlation between two maps over a fixed area to a continuously varying local measure of the correspondence between the spatial patterns in two fields. As detailed in the appendix, this is accomplished by using a smooth localizing function in order to define the spatial means and the spatial variances of both fields as well as their covariance. The correlation field between simulated and ECMWF 200-hPa zonal wind u is presented for the normal ensemble in Fig. 4a and for the warm ensemble in Fig. 4b. (For both ensembles, the ensemble correlation was calculated using the ensemble-averaged covariances and variances that enter into the definition of the correlation.) The local correlation for the normal winters is low, exceeding 0.3 only in the tropical Pacific and equatorward of 40°N in the PNA region. However, the warm ensemble correlation field reaches a maximum of 0.8 just east of the date line on the equator and exceeds 0.6 in a broad region over the central and eastern Pacific and over western North America. The area enclosed by the 0.5 contour covers the entire PNA region and extends almost to 30°S. The dramatic difference between the correlation fields in El Niño and normal winters indicates the dominant role of boundary forcing in seasonal predictability for this GCM. Similar results are obtained for the correlation field of the 200-hPa geopotential height field z (not shown).

Since our main interest is the behavior of the transients in the storm track regions, the shift in the Pacific jet during El Niño winters is particularly germane. The difference (warm minus normal) between the ensemble averaged 300-hPa height field z is shown in Figs. 5a (6a) from the ECMWF analyses (GCM) and the corresponding difference in u in Figs. 5b (6b). The strong minimum in z anomaly in the North Pacific corresponds to cyclonic circulation in accord with the classic picture of the midlatitude response to El Niño (Horel and Wallace 1981). The meridional gradient of this anomaly gives the anomaly in the zonal wind u, which has a

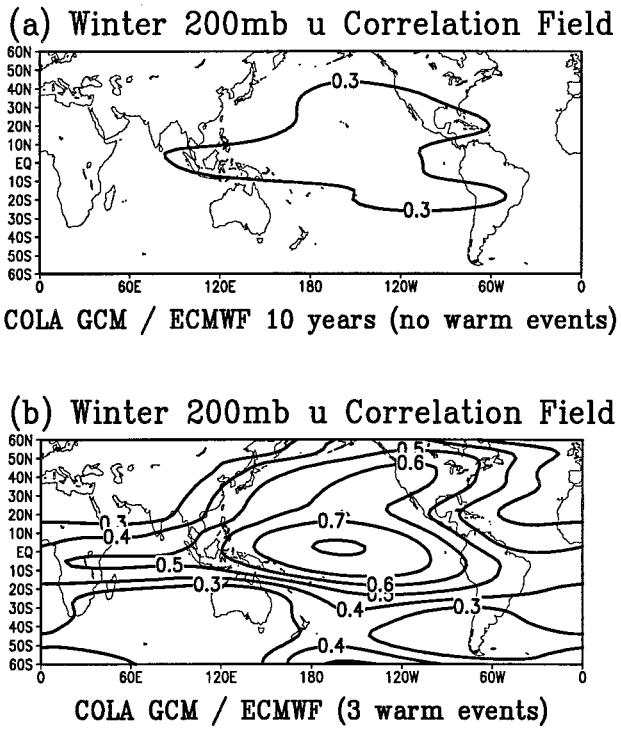

FIG. 4. Correlation field of 200-hPa zonal wind u. See text for definition. (a) Normal ensemble; (b) warm ensemble. Contour interval is 0.1, with contours less than 0.3 not plotted.

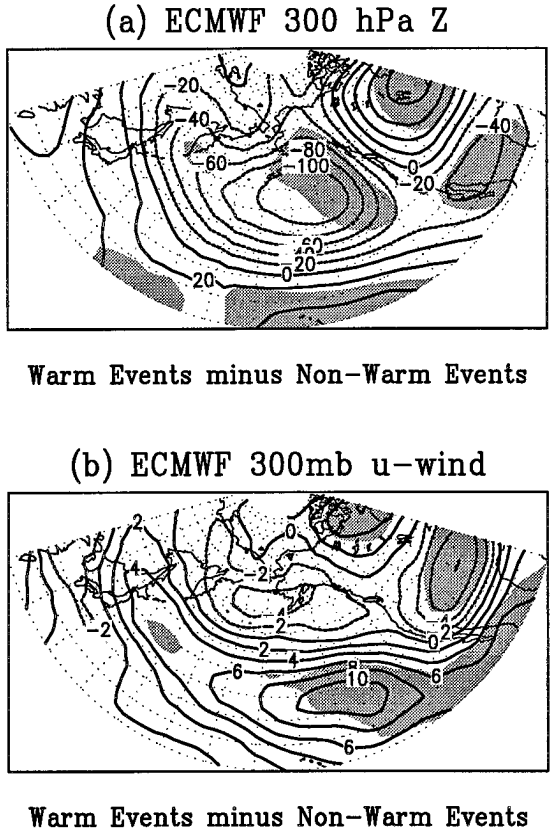

FIG. 5. Difference between warm and normal ensembles for ECMWF. (a) 300-hPa geopotential height z. (b) 300-hPa zonal wind u. Shading indicates significance at the 95% level. In this and all subsequent figures, a polar stereographic projection is used to show the region from latitude 20°N to 80°N, longitude 120°E to 270°E. Contour is 10 m in (a), 2 m s^{-1} in (b).

strong maximum at about 40°N in the eastern Pacific. This positive anomaly extends eastward all the way across Mexico (Fig. 5b for the ECMWF results, Fig. 6b for the GCM), and is accompanied by a decrease in u farther east (over central North America) and farther north in the Pacific in both the analyses and the GCM. Taken together with the position of the mean upper-level jet, these changes indicate an eastward extension and southward shift in the jet during El Niño winters. Note that the large positive anomaly in the eastern Pacific is generally significant at the 95% confidence level (as indicated by the shaded area) in the ECMWF results but less so in the GCM. The decrease in u over the central United States and the increase over Mexico are significant in both analyses and GCM, but the magnitude of the change is much smaller in the GCM. Noteworthy in Figs. 5b and 6b are the positive anomalies at the *western* edge of the storm track. This enhancement occurs off northern Japan at about 40°N in the analyses (and is not statistically significant), but occurs farther south (latitude 25°N) in the GCM where it is significant.

The strong positive anomaly seen in Figs. 5 and 6 occurs in an area in which the GCM already has a large systematic error in the zonal wind, as indicated in Fig. 7 for both z and u at the 300-hPa level. (The systematic error is defined as the difference between the GCM's winter climatology and that of the ECMWF analyses for the 13 winters 1980/81 through 1992/93.) A detailed analysis of the COLA GCM's response to El Niño SST forcing utilizing a linearized version of the GCM in which the basic state retains asymmetric (eddy) components has shown that the systematic error of the model is one of the prime causes of errors in the anomalous winter stationary waves during El Niño (Peng 1995).

5. Transients and storm track dynamics

The regions of maximum transient variance on timescales of 3–10 days (hereafter referred to as high frequency) that extend eastward off the coasts of Asia and North America and well into the major ocean basins are characterized by strong baroclinic development (Blackmon et al. 1977; Simmons and Hoskins 1978; Lau 1978). The location of these broad maxima over the Atlantic and Pacific Oceans, which we refer to as storm tracks[1] is closely tied to the regions of maximum baro-

[1] We follow common usage. A better term, however, would be "baroclinic waveguides," as suggested by Wallace et al. (1988).

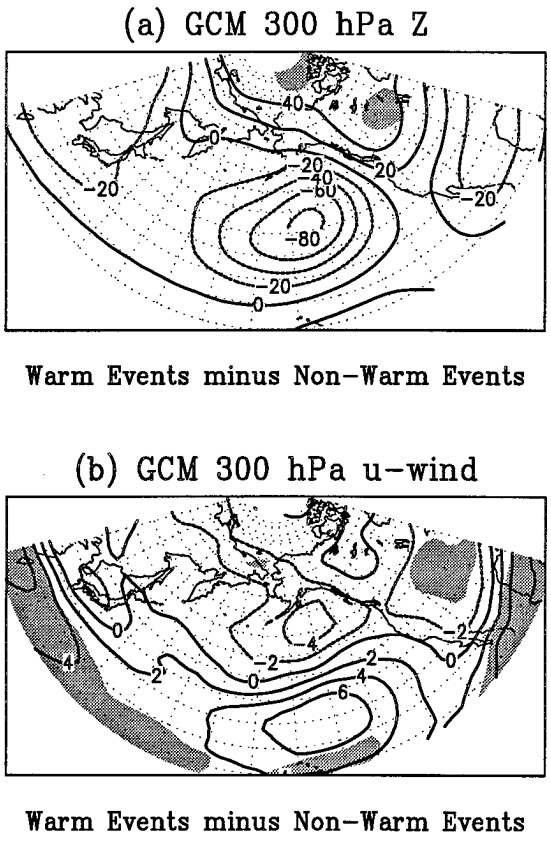

FIG. 6. Difference between warm and normal ensembles for the GCM; (a) 300-hPa geopotential height z and (b) 300-hPa zonal wind u. Shading indicates significance at the 95% level. Contour interval is 10 m in (a), 2 m s^{-1} in (b).

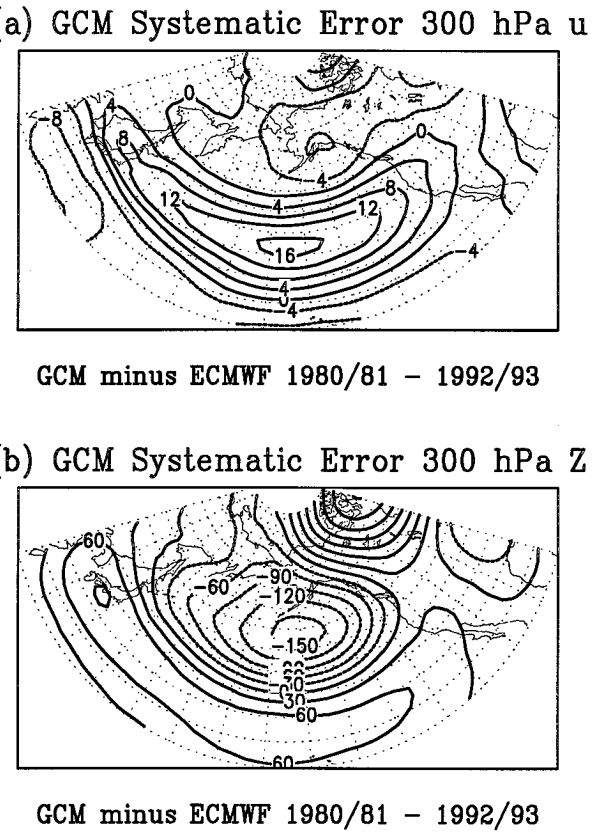

FIG. 7. GCM Winter systematic error in (a) 300-hPa zonal wind u and (b) 300-hPa geopotential height z. Contour interval is 2 m s^{-1} in (a) and 10 m in (b).

clinicity (and hence the major oceanic subtropical jets) and demonstrates interannual variability that is linked to that of the mean flow (Lau 1988). While the mean flow gradients are responsible for enhancing the transients through basically linear baroclinic processes in the upstream (western) portions of the storm tracks (e.g., Simmons and Hoskins 1978; Frederiksen 1979), the downstream (eastern) portion of the storm tracks is characterized by more barotropic processes associated with the maturity and decay of the transient systems (Simmons and Hoskins 1978; Lim and Wallace 1991). Overall, the transients exert a strong feedback on the mean flow via the competition between (i) the transient heat flux that tends to destroy the baroclinicity (decrease the vertical shear) and (ii) the transient vorticity flux that tends to reinforce the mean flow by accelerating the upper-level jet (Lau and Holopainen 1984).

Given the large changes in the upper-level u seen in the last section to be associated with warm events, we would expect to see concomitant changes in the transient–mean flow interaction. In this section we examine the differences in transient statistics between the warm ensemble and the normal ensemble with the goal of illustrating both components of this interaction.

The influence of the upper-level transients in the central and eastern Pacific in extending the Pacific jet toward the east of the oceanic basin during El Niño has been well documented by Held et al. (1989), Hoerling and Ting (1994), and Peng (1995). The tendency in u obtained from the tendency in vorticity that is implied by the convergence of the high-frequency transient vorticity flux is shown for the ECMWF analyses and the GCM in Fig. 8. (The method used to time-filter the data is given in the appendix.) The tendency in u was computed for all winters; the average over all winters is shown in Fig. 8a (Fig. 8c) for the analyses (GCM), while the difference between the warm and normal ensemble averages is shown in Fig. 8b (Fig. 8d).

Climatologically, the implied zonal flow acceleration in the ECMWF analyses (Fig. 8a) is maximum in the western Pacific and decays east of the date line (although it begins to grow again over the North American continent). During warm events, the change in mean flow acceleration (Fig. 8b) is in the sense of an eastward and equatorward enhancement of the jet. (The tendency anomalies are very similar in overall structure to the actual anomalies shown in Fig. 5b.) Both the acceleration in the eastern Pacific and at least the most intense deceleration (in the Gulf of Alaska and over Southern Cal-

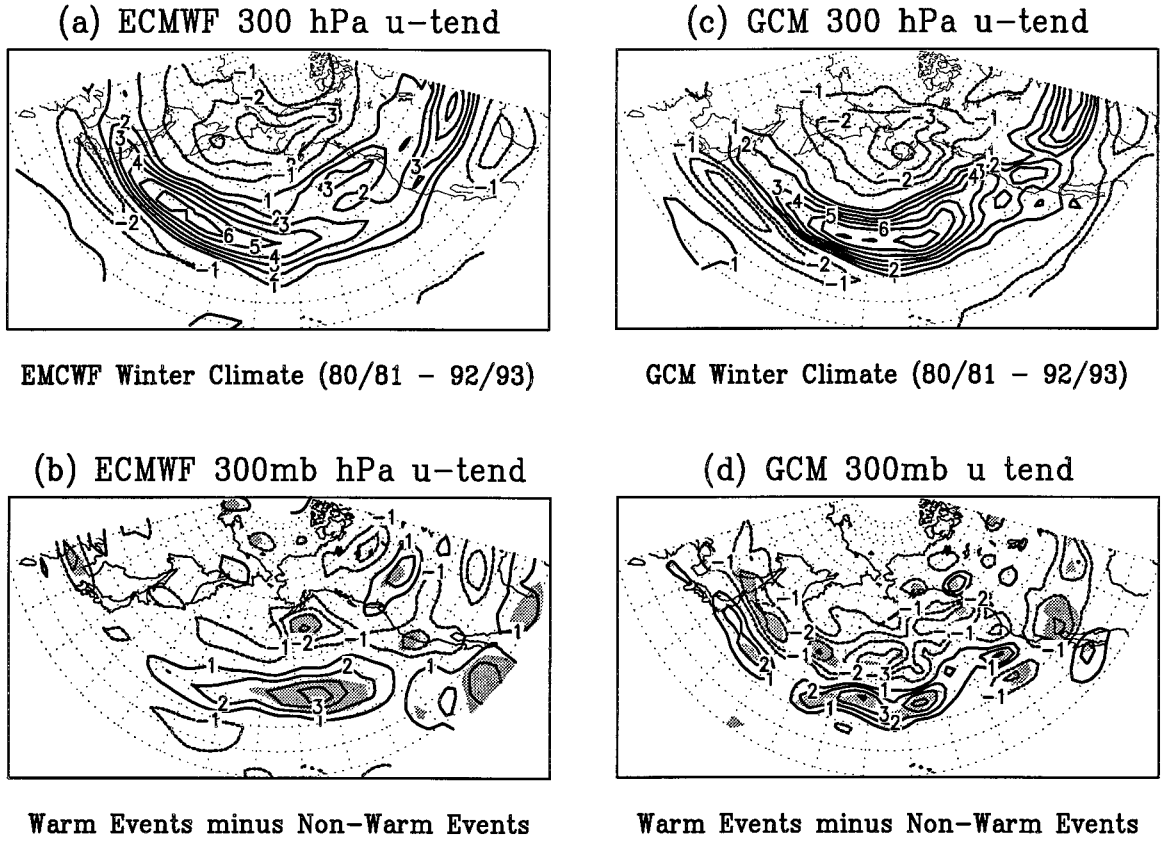

FIG. 8. Tendency in mean zonal wind u implied by the convergence of high-frequency vorticity flux at 300 hPa (see text for details). (a) Winter climatology from ECMWF analyses. (b) Difference between warm and normal ensembles from ECMWF analyses. (c) GCM climatology. (d) Difference between warm and normal ensembles from GCM. Contour interval is 1 m s^{-1} day^{-1} throughout. Shading in (b) and (d) indicates significance at the 95% level.

ifornia) are statistically significant (indicated by shading in Fig. 8 and all the remaining figures in this section).

The mean pattern of zonal flow acceleration in the GCM (Fig. 8c) illustrates a recurrent error in the COLA GCM, namely, the eastward displacement of the storm track (here seen in the vorticity flux convergence). The *anomaly* in tendency, however, agrees rather well with the ECMWF results, although due to the mean error it is the equatorward shift that is more prevalent than the eastward extension (however, note the small but significant area of positive tendency anomaly off the coast of California.) At the 200-hPa level (not shown), the ECMWF results are basically unchanged, while the GCM anomaly is fairly weak although the pattern is similar to that at 300 hPa.

A measure of the storm track activity that is weighted toward the more mature eddies, those with a predominantly barotropic structure, is the high-frequency transient kinetic energy (TKE). Again the average over all winters is shown in Fig. 9a (analyses) and Fig. 9c (GCM), while the warm minus normal anomalies appear in Figs. 9b and 9d. Comparison of the ECMWF and GCM climatologies (Figs. 9a and 9c) indicates that the more mature eddies are well positioned in the GCM, but are too weak in a statistical sense. The ECMWF warm anomalies (Fig. 9b) show a weakening of activity in the North Pacific, accompanied by an enhancement in a band that extends from the central Pacific (latitudes 35°–40°) eastward and southward clear across Mexico. Much of this band is significant (indicated by the shading), and the value of the t-statistic (not shown) exceeds 4.0 over western Mexico and the eastern subtropical Pacific. (As noted in the appendix, a value of 2.2 already implies significance at the 95% level.)

The simulated change in high-frequency TKE (Fig. 9d) shows broad agreement in terms of the overall pattern (suppression to the north, enhancement to the south and east) and in terms of area of significance, but the magnitude of the change is quite weak, especially the enhancement in the eastern Pacific. Note the area of significantly higher TKE in the GCM results during El Niño in the subtropical western Pacific (latitude 30°N), in accord with the enhancement of the zonal wind in this region (Fig. 6a).

Another measure of the degree of actively developing wintertime eddies over the oceans is the diabatic heating due to latent heat release. While the time-mean heating does not directly discriminate on the basis of timescale,

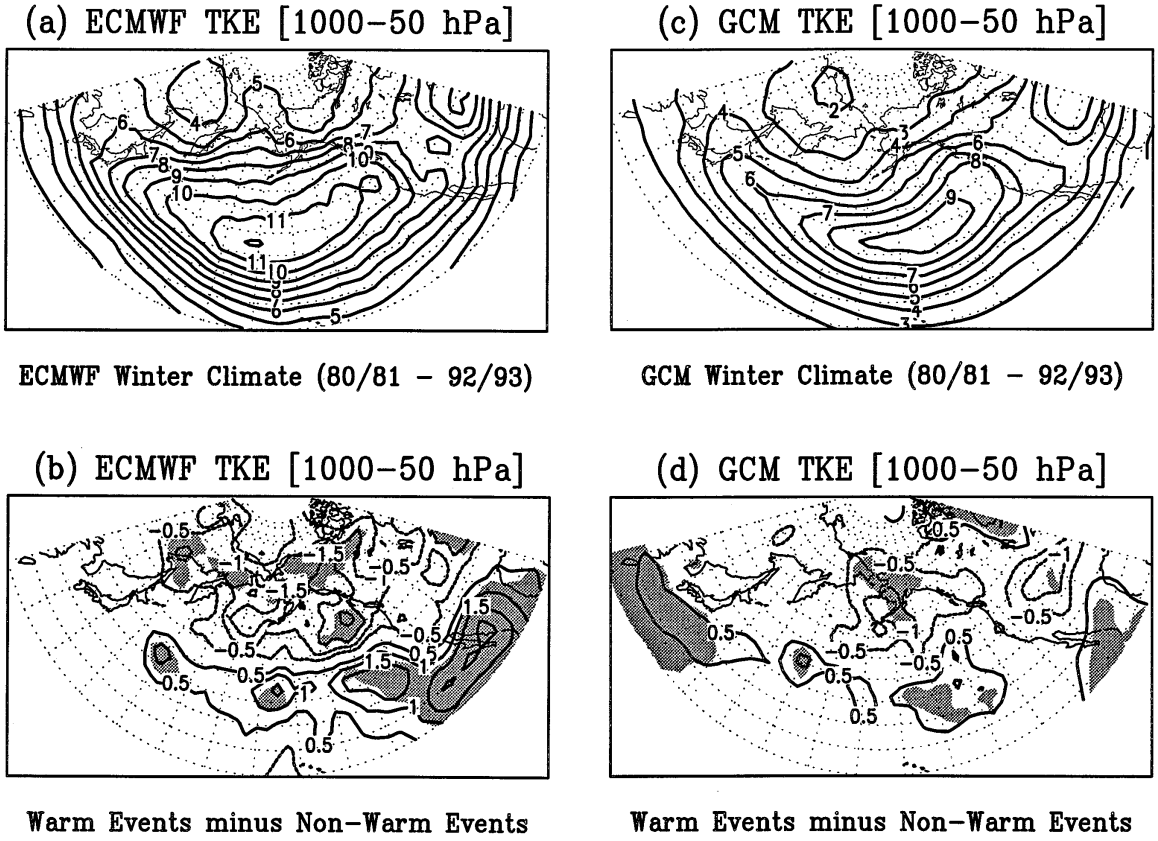

FIG. 9. High-frequency transient kinetic energy integrated between 1000 and 50 hPa (see text for details). (a) Winter climatology from ECMWF analyses. (b) Difference between warm and normal ensembles from ECMWF analyses. (c) GCM climatology. (d) Difference between warm and normal ensembles from GCM. Contour interval is 1.0×10^5 J m^{-2} in (a) and (c), 0.5×10^5 J m^{-2} in (b) and (d). Shading in (b) and (d) indicates significance at the 95% level.

we expect areas of strong latent heating (and precipitation) over the oceans to be closely related to both the dynamics and the maintenance of the storm tracks themselves (Hoskins and Valdes 1990). The climatological precipitation from the MSU data (GCM) is seen in Fig. 10a (10c). The maximum extending eastward off the coast of Asia delineates the upstream portion of the storm track very clearly. The maximum along the west coast of Canada and Alaska occurs in an area in which low-frequency transients dominate (not shown). The warm minus normal anomaly (Fig. 10d) is dominated by the positive anomaly east of the date line that is consistent with a downstream extension of the storm track, but which is statistically significant only in a small region. The negative anomalies in the North Pacific are completely consistent with those of TKE, as are the positive anomalies at 30°N at the longitude of Japan.

The high-frequency meridional flux of sensible heat in the lower troposphere, which provides another diagnostic of the developing eddies in the storm track, is shown (averaged vertically from 1000 to 500 hPa) in Figs. 11 and 12. The ECMWF (GCM) winter climatology is given in Fig. 11a (Fig. 12a) and the warm minus normal anomaly in Fig. 11b (Fig. 12b). The climatologies depict a smooth and very well defined storm track. The shift of the maximum toward the central Pacific in the GCM climatology (Fig. 12a) is another indication of the systematic error referred to previously. The anomaly maps clearly indicate both a small (but significant) increase in the extreme western Pacific (130°E) and a broad region of positive heat flux anomalies extending from northern Japan eastward and (slightly equatorward) past the date line. This is accompanied by a broad region of negative anomalies over the high-latitude central Pacific. The whole picture is one of a storm track that is extended and shifted towards the equator. The significant increase near Japan in the GCM is consistent with increases there in the TKE and diabatic heating.

The observed storm tracks are a self-maintaining entity in which rapidly growing baroclinic disturbances do *not* effectively neutralize the localized baroclinicity in the mean state (Hoskins and Valdes 1990) as would be expected on the basis of dry dynamics alone (Simmons and Hoskins 1978). We thus would expect the baroclinicity to show differences between warm and normal ensembles consistent with those presented above. A

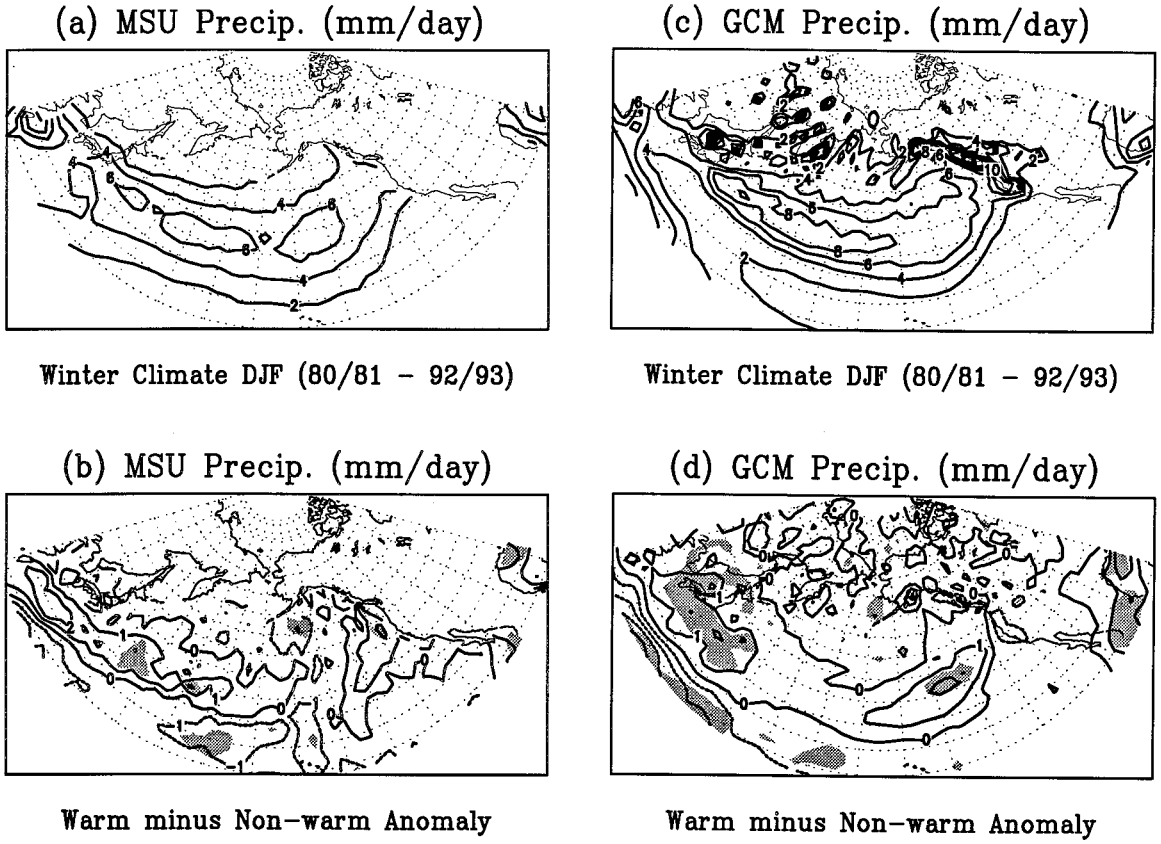

FIG. 10. (a) Winter precipitation climatology from MSU data. (b) Difference between warm and normal ensemble MSU precipitation. (c) Winter precipitation climatology from GCM. (d) Difference between warm and normal ensemble GCM precipitation. Contour interval is 2 mm/day in (a) and (c), 1 mm/day in (b) and (d). Shading in (b) indicates significance at the 95% level.

measure of this baroclinicity is the inverse square root of the Richardson number $Ri^{-1/2}$, which is the ratio of the vertical wind shear to the square root of the buoyancy frequency (Nakamura 1992). [We calculated $Ri^{-1/2}$ separately for the 850–700 hPa layer and the 700–500 hPa layer, using the formulation of Nakamura (1992). We generally found the 700–500 hPa layer to show larger values for both ensemble means and differences, and will present only this layer.] This measure is shown for the normal ensemble, the warm ensemble, and their difference for the ECMWF analyses (GCM) in Figs. 13 (14). The systematic error of the GCM in extending the storm tracks too far east is seen by comparing the locus of large values (greater than of 0.3) of $Ri^{-1/2}$ in Figs. 13a and 14a. In the analyses, the largest differences in $Ri^{-1/2}$ track the differences in sensible heat flux and TKE fairly well from the Japanese coast eastward past the date line. Interestingly, this coherent pattern of increased $Ri^{-1/2}$ is not significant statistically until well out in the storm track (~210°E). Further eastward it diminishes somewhat in value, but retains its significance clear across Mexico, and is here closely tied to the increase seen in TKE (Fig. 9b) during the warm events.

The GCM baroclinicity (Fig. 14) differs from the analyzed baroclinicity in the western Pacific in that the warm minus normal anomaly is shifted about 15° equatorward, indicating that it is the southern flank of the simulated baroclinic region that is most changed during El Niño. This (significant) change west of the date line is closely tied to large high-frequency transient heat flux, TKE, and enhanced precipitation anomalies during El Niño, which all tend to be more prevalent in the far western Pacific and to lie to the south of the corresponding ECMWF quantities. East of the date line, the GCM and ECMWF fields agree better in terms of the location of the maxima at about 205°E and again over Mexico, although the GCM baroclinicity has a much sharper minimum between these maxima.

An examination of the components of $Ri^{-1/2}$, namely the vertical wind shear and the square root of the buoyancy frequency, indicated that the anomalies in $Ri^{-1/2}$ are dominated by those in the vertical wind shear. The increase in the shear seen in the Pacific to the east of the date line is completely consistent with the location of the greatest tropical warming seen during warm events in Yulaeva and Wallace (1994) via the thermal wind relation (see their Fig. 22).

Since growing baroclinic transients transport sensible

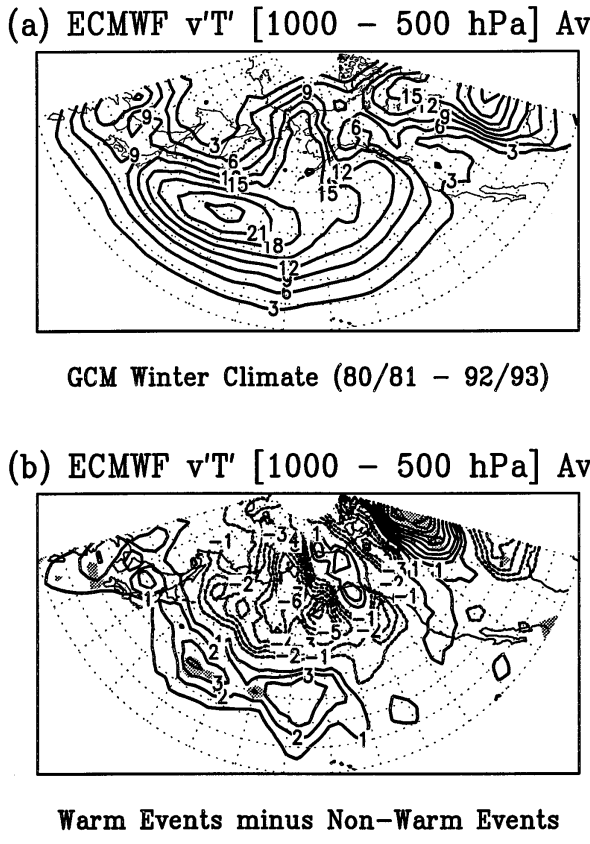

FIG. 11. High-frequency meridional flux of sensible heat from ECMWF analyses, vertically averaged from 1000 to 500 hPa. (a) Winter climatology. (b) Difference between warm and normal ensemble. Contour interval is 3 m s^{-1} K in (a), 1 m s^{-1} K in (b). Shading in (b) indicates significance at the 95% level.

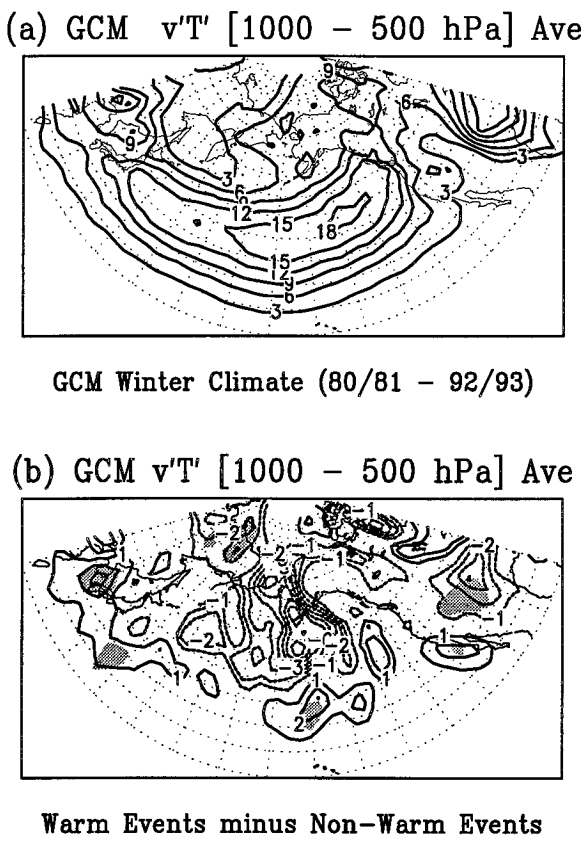

FIG. 12. High-frequency meridional flux of sensible heat from the GCM, vertically averaged from 1000 to 500 hPa. (a) Winter climatology. (b) Difference between warm and normal ensemble. Contour interval is 3 m s^{-1} K in (a), 1 m s^{-1} K in (b). Shading in (b) indicates significance at the 95% level.

heat upwards (see Lim and Wallace 1991 for a review), we examine the total transient vertical flux of sensible heat as a final check on the consistency of the shifts in storm track activity. The climatology of this flux at 700 hPa is given for the analyses (GCM) in Fig. 15a (Fig. 16a) and the corresponding warm minus normal anomalies in Fig. 15b (Fig. 16b). The position of the climatological maximum is quite similar to that of the meridional heat flux for both the analyses and the GCM. The ECMWF anomalies, while rather noisy, consistently show an increased heat transport (and in some small regions significantly so) downstream and slightly equatorward of the climatological storm track. The GCM results are less clear, however, for while the anomalies (Fig. 16b) again indicate an equatorward and downstream shift, the magnitudes are low.[2]

[2] The GCM data were sampled once per day, while the analyses were sampled twice per day. The extent to which the transient vertical heat flux, an intrinsically intermittent quantity, is sensitive to sampling errors is not well known.

6. Summary and discussion

During the El Niño events studied here, the dramatic eastward extension of the warm Pacific SSTs is reflected in corresponding deep tropical diabatic heating anomalies in the GCM. Based on these heating anomalies, we have defined warm and normal ensembles of winters. The warm minus normal ensemble difference of various midlatitude statistics is used to define the El Niño response both in the GCM and the analyses. Our emphasis is on the response seen in those second-order statistics that are indicators of the various regimes of the storm tracks. Inclusion of the more baroclinic regions of the storm tracks as well as the barotropic (downstream) region in the discussion of warm events goes beyond previous work.

The transient second-order statistics presented (high-frequency kinetic energy, meridional heat flux, vertical heat flux, and vorticity flux convergence), in conjunction with examination of the anomalies in seasonal mean u-wind, precipitation, and $\mathrm{Ri}^{-1/2}$, show an eastward and equatorward shift of the entire storm track complex in the GCM and the ECMWF analyses. The shift is con-

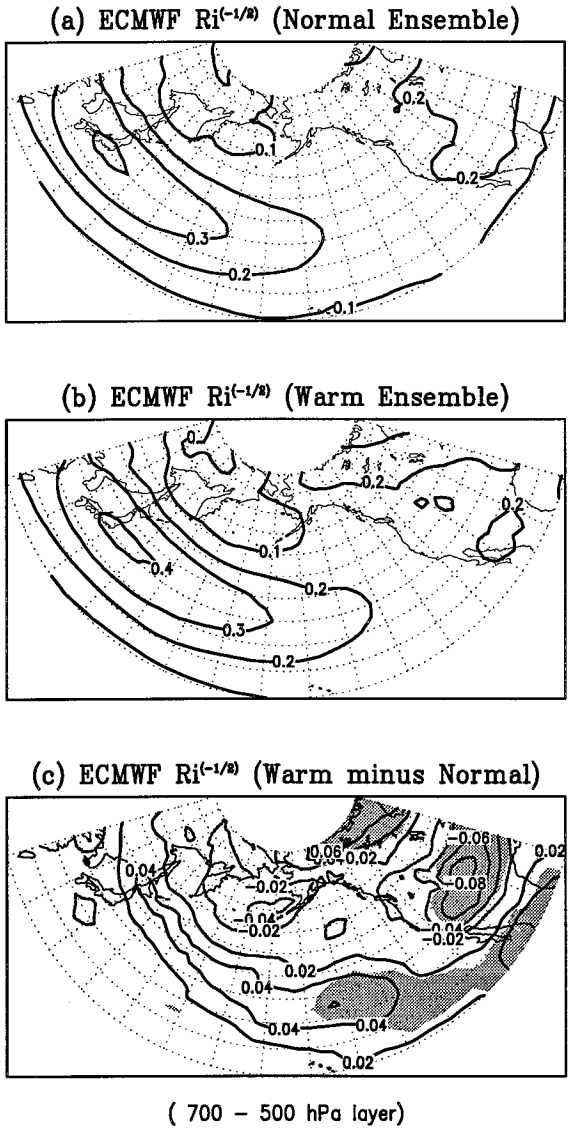

FIG. 13. The dimensionless quantity $Ri^{-1/2}$ calculated from the ECMWF analyses for the 700-hPa–500-hPa layer (see text for details). (a) Normal ensemble. (b) Warm ensemble. (c) Warm minus normal ensemble. Contour interval is 0.1 for (a) and (b), 0.02 for (c). Shading in (c) indicates significance at the 95% level.

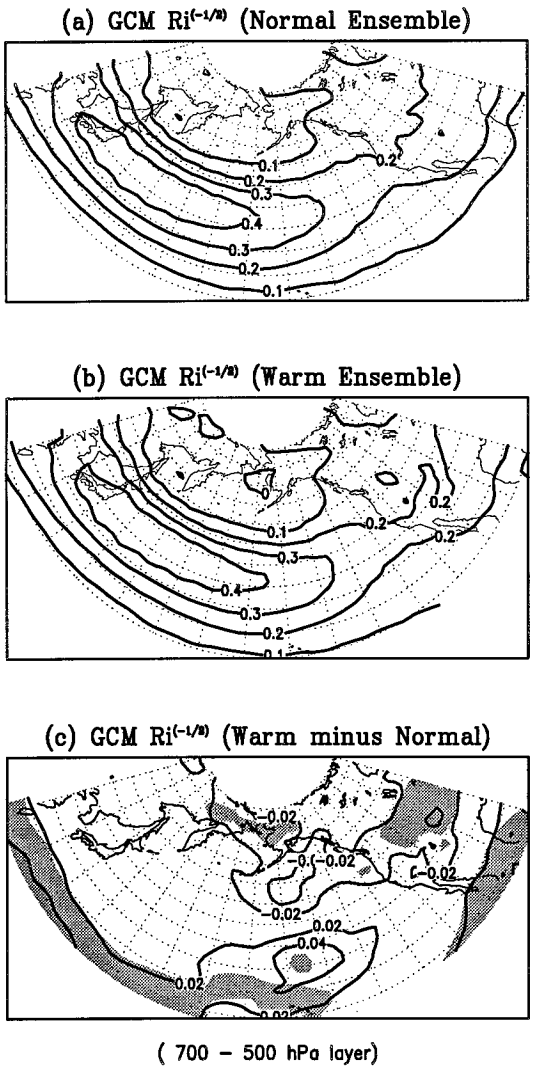

FIG. 14. The dimensionless quantity $Ri^{-1/2}$ calculated from the GCM for the 700-hPa–500-hPa layer (see text for details). (a) Normal ensemble. (b) Warm ensemble. (c) Warm minus normal ensemble. Contour interval is 0.1 for (a) and (b), 0.02 for (c). Shading in (c) indicates significance at the 95% level.

sistent with the increased midlatitude shear during El Niño that accompanies the overall tropical warming.

While the GCM shift in the storm track has strong similarities to that seen in the analyses, the GCM's large systematic error in the mid Pacific causes a large, erroneous eastward shift in the *normal* storm track complex compared to the analyses, as seen in the climatological u-wind and in $Ri^{-1/2}$, as well as in the transient fluxes of heat and vorticity. Since the form of the systematic error in the Pacific is similar to the observed El Niño anomaly pattern, it is perhaps not surprising that the GCM anomaly pattern is too weak. A more complete discussion of the relationship between the systematic error and the response to El Niño is given in Peng (1995).

The GCM also shows a spurious tendency to move the storm track equatorward in the far western Pacific, seen for example in the anomalies of u-wind, high-frequency kinetic energy, precipitation, sensible heat flux, and in $Ri^{-1/2}$. The cause of this problem awaits further research.

The equatorward shift and eastward extension of the center of high-frequency activity is seen both in quantities that measure the baroclinic aspects of developing disturbances (meridional and vertical sensible heat fluxes, precipitation) and in those emphasizing barotropic aspects of the flow (vorticity flux convergence and TKE). The change in the heat fluxes in the central Pacific

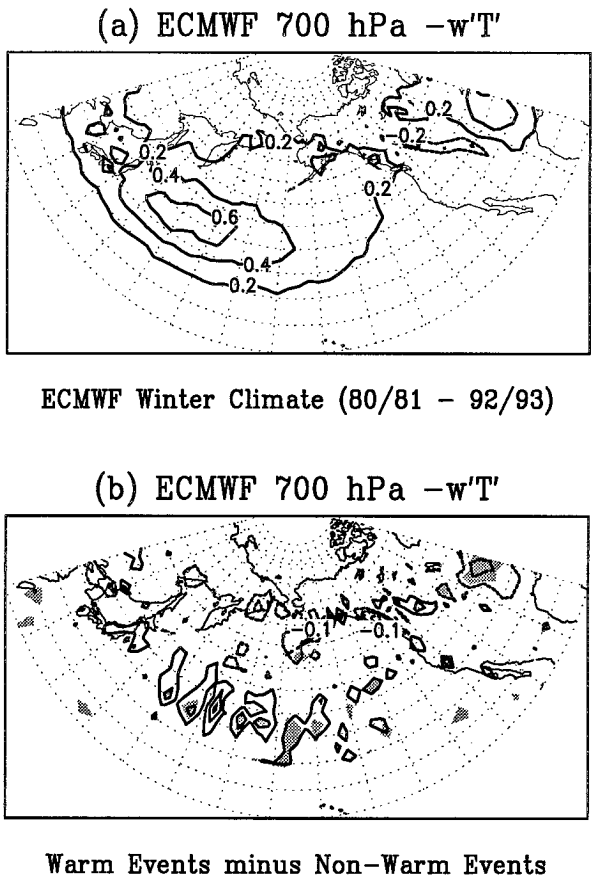

FIG. 15. Transient vertical flux of sensible heat from ECMWF analyses at 700 hPa. (a) Winter climatology. (b) Difference between warm and normal ensemble. Contour interval is 0.2 Pa/sec in (a), 0.1 Pa/sec in (b). Shading in (b) indicates significance at the 95% level.

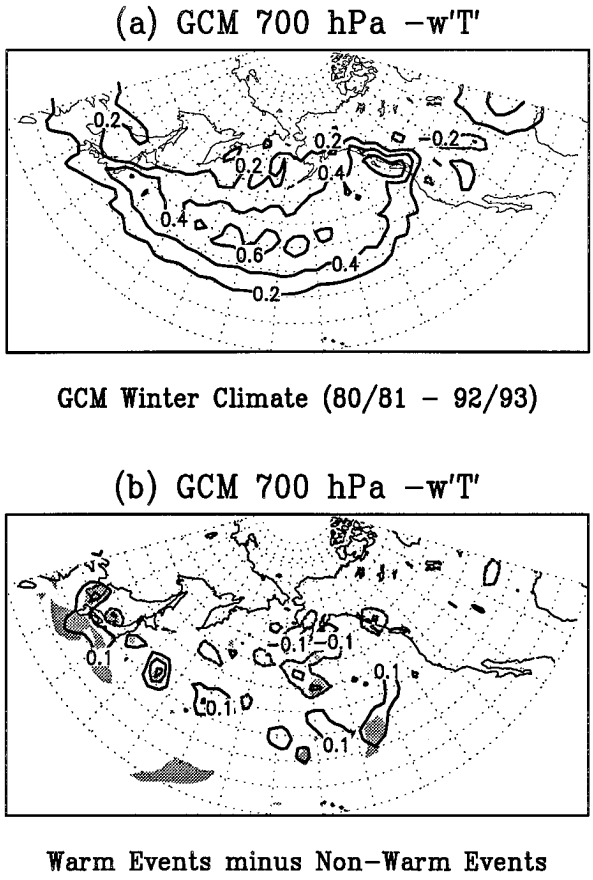

FIG. 16. Transient vertical flux of sensible heat from the GCM at 700 hPa. (a) Winter climatology. (b) Difference between warm and normal ensemble. Contour interval is 0.2 Pa/sec in (a), 0.1 Pa/sec in (b). Shading in (b) indicates significance at the 95% level.

is interpreted as an enhancement in the zone of baroclinic development in the mid Pacific during warm events, consistent with the overall warming of the Tropics and hence the increased midlatitude vertical shear and baroclinity.

Changes in the TKE are largest at upper levels and in the eastern Pacific, downstream of the manifestation of the storm track at lower levels. Several dynamical processes may contribute to the enhancement of the more barotropic eddies here during warm events. One is simply that the normal downstream barotropic response to baroclinic development [Simmons and Hoskins (1978), and from another perspective, Lim and Wallace (1991)] has been shifted in response to the shift in the zone of baroclinic development. Another competing mechanism is the enhancement of barotropic instability (Simmons et al. 1983) associated with an enhanced jet in the eastern Pacific during warm events. The most rapidly growing mode calculated by Simmons et al. has an *e*-folding time of about 1 week, and so would be barely captured by our high-frequency filter (~3–10 days). However, the possibility of a baroclinic component to these predominantly barotropic instabilities is raised by the appearance of positive anomalies in both horizontal and vertical heat fluxes in the eastern Pacific.

The enhancement of TKE over Mexico and the positive GCM anomaly of rainfall during warm events not only agree well with observations (Cavazos and Hastenrath 1990), but argue that both baroclinic dynamics (possibly small scale) and orographic forcing may be important in this region.

The relationships between the anomalies in the (seasonal) mean flow field and the high-frequency eddies that define the storm track have been studied here in the context of ENSO. Similar synoptic scale–mean flow relationships have been well documented from a purely midlatitude point of view by Lau (1988). In that paper (based on data from 1953 to 1981), empirical orthogonal functions (EOFs) of the storm tracks (defined solely on the basis of the high-frequency component of the 500-hPa height field) were used to define the basic patterns of variability. By correlating the time-dependent coefficients of each EOF with monthly mean anomalies, Lau obtained associated stationary wave patterns. Of the two overall changes in the storm track configuration we find to be associated with ENSO, the equatorward shift and

eastward extension, only the former is captured in Lau's analysis (see his EOF 2, Fig. 2b). The pattern of monthly mean height anomalies that is associated with that pattern (Lau's Fig. 4b) resembles our warm minus cold height difference only very roughly, both of them showing some degree of resemblance to the PNA pattern of Wallace and Gutzler (1981).

The discrepancy between our study and that of Lau can be understood both as a reflection of the different periods of time used and the fundamental distinction between modes of variability associated with external forcing and those which characterize the total (internal plus external) set of fluctuations.

Acknowledgments. This work was supported by the Office of Global Programs of the National Oceanic and Atmospheric Administration under Grants NA89AA-D-AC204 and NA26 GP0101-01, and by the Climate Dynamics Program of the National Science Foundation under Grant ATM 9321354. Computer time was provided by the Atmospheric Model Intercomparison Program (AMIP) and by the Pittsburgh Supercomputing Center. We wish to thank Ms. Mary Ann Huntley and Ms. Qiulian Yang for able programming assistance.

APPENDIX

Data Analysis

a. Correlation field

The correlation field compares the local spatial structure of two fields, F and G. At any point it is simply the pattern correlation between localized versions of F and G, where the localization is accomplished by multiplying the fields by a two-dimensional Gaussian envelope. We begin by defining the (local) mean of F as

$$\langle F\rangle(\lambda_0, \phi_0) = \int\int F \exp\left[-\left(\frac{\lambda - \lambda_0}{W_1}\right)^2\right] \exp\left[-\left(\frac{\phi - \phi_0}{W_2}\right)^2\right] d\mu\, d\lambda, \quad \text{(A1)}$$

where $\mu = \sin\phi$, λ_0 and ϕ_0 are the longitude and latitude at the center of the local region, and the parameters W_1 and W_2 define the longitudinal and latitudinal width.

Given the definition of the angular brackets implied in Eq. (A1), we can define the covariance between F and G as

$$C_{F,G} = \langle (F - \langle F\rangle)(G - \langle G\rangle)\rangle \quad \text{(A2)}$$

and the spatial variance as

$$V_F = \langle (F - \langle F\rangle)^2\rangle. \quad \text{(A3)}$$

Finally, letting S_F denote the square root of V_F, we can define the local correlation H as

$$H_{F,G} = C_{F,G}/(S_F S_G). \quad \text{(A4)}$$

In practice the integral in Eq. (A1) is done over only those latitudes and longitudes for which the Gaussian weight is nonnegligible. For example, if we restrict the range of integration so that $|\lambda - \lambda_0| \le 2W_1$ and $|\phi - \phi_0| \le W_2$, then for global fields the means $\langle F\rangle$ and $\langle G\rangle$ are defined only for the latitudes $-(\pi/2 - W_2) \le \phi_0 \le (\pi/2 - W_2)$. Application of the integral again is necessary to obtain the covariance and variances as in Eq. (A2) and the final results are then only defined for $-(\pi/2 - 2W_2) \le \phi_0 \le (\pi/2 - 2W_2)$.

A note on the choice of W_1 and W_2: Sensible choices depend very much on the desired application, since these parameters can be intrepreted as a dimensionless wavelength. We have found that the values $W_1 = \pi/3$ and $W_2 = \pi/12$ are satisfactory for the anomaly fields of seasonal mean heights and winds at upper levels.

b. Statistical significance

We apply the t statistic to interpret the significance of the difference between the means of two samples in the usual way (Snedecor and Cochran 1978). The warm ensemble has three members and the normal ensemble 10 members. The 95% level of significance is associated with a value of t of 2.20.

c. Time filtering

In order to obtain the time-filtered variances and covariances presented in the paper, we have used the method of Lorenz (1979). This method simply computes the (co)variances within bands. The first band corresponds to the (co)variance of daily means within 2-day periods, the second to the (co)variance of 2-day means within 4-day periods, and so forth, ending with the (co)variance of 64-day means within the 128-day season. The frequency response corresponding to each band is rather broad (Trenberth 1981). Summing the first three bands gives the (co)variance including roughly periods of 3–10 days.

REFERENCES

Barnett, T. P., 1995: Monte Carlo climate forecasting. *J. Climate,* **8,** 1005–1022.

Bjerknes, J., 1966: A possible response of the atmospheric Hadley circulation to equatorial anomalies of ocean temperature. *Tellus,* **18,** 820–829.

——, 1969: Atmospheric teleconnections from the equatorial Pacific. *Mon. Wea. Rev.,* **97,** 163–172.

Blackmon, M. L., J. M. Wallace, N.-C. Lau, and S. L. Mullen, 1977: An observational study of the Northern Hemisphere wintertime circulation. *J. Atmos. Sci.,* **34,** 1040–1053.

——, J. E. Geisler, and E. J. Pitcher, 1983: A general circulation model study of January climate anomaly patterns associated with interannual variation of equatorial Pacific sea surface temperatures. *J. Atmos. Sci.,* **40,** 1410–1425.

Cavazos, T., and S. Hastenrath, 1990: Convection and rainfall over Mexico and their modulation by the Southern Oscillation. *Int. J. Climatol.,* **10,** 377–386.

Fennessy, M. J., and J. Shukla, 1988: Numerical simulation of the

atmospheric response to the time-varying El Niño SST anomalies during May 1982 through October 1983. *J. Climate,* **1,** 195–211.
——, L. Marx, and J. Shukla, 1985: General circulation model sensitivity to 1982–83 equatorial Pacific sea surface temperature anomalies. *Mon. Wea. Rev.,* **113,** 858–864.
Frederiksen, J.S., 1979: The effects of long planetary waves on the regions of cyclogenesis: Linear theory. *J. Atmos. Sci.,* **36,** 195–204.
Gates, W. L., 1992: AMIP: The Atmospheric Model Intercomparison Project. *Bull. Amer. Meteor. Soc.,* **73,** 1962–1970.
Held, I. M., S. W. Lyons, and S. Nigam, 1989: Transients and the extratropical response to El Niño. *J. Atmos. Sci.,* **46,** 163–174.
Hoerling, M. P., and M. Ting, 1994: Organization of extratropical transients during El Niño. *J. Climate,* **7,** 745–766.
Horel, J. D., and J. M. Wallace, 1981: Planetary-scale atmospheric phenomena associated with the Southern Oscillation. *Mon. Wea. Rev.,* **109,** 813–829.
Hoskins, B. J., and D. J. Karoly, 1981: The steady linear response of a spherical atmosphere to thermal and orographic forcing. *J. Atmos. Sci.,* **38,** 1179–1196.
——, and P. J. Valdes, 1990: On the existence of storm tracks. *J. Atmos. Sci.,* **47,** 1854–1864.
Kinter, J. L., III, J. Shukla, L. Marx, and E. K. Schneider, 1988: A simulation of the winter and summer circulations with the NMC global spectral model. *J. Atmos. Sci.,* **45,** 2486–2522.
Kok, C. J., and J. D. Opsteegh, 1985: Possible causes of anomalies in seasonal mean circulation patterns during the 1982–83 El Niño event. *J. Atmos. Sci.,* **42,** 677–694.
Kumar, A., and M. P. Hoerling, 1995: Prospects and limitations of seasonal GCM predictions. *Bull. Amer. Meteor. Soc.,* **76,** 335–345.
Lau, N.-C., 1978: On the three-dimensional structure of the observed transient eddy statistics of the Northern Hemisphere wintertime circulation. *J. Atmos. Sci.,* **35,** 1900–1923.
——, 1985: Modeling the seasonal dependence of the atmospheric response to observed El Niños in 1962–76. *Mon. Wea. Rev.,* **113,** 1970–1996.
——, 1988: Variability of the observed midlatitude storm tracks in relation to the low-frequency changes in the circulation pattern. *J. Atmos. Sci.,* **45,** 2718–2743.
——, and E. O. Holopainen, 1984: Transient eddy forcing of the time-mean flow as identified by geopotential tendencies. *J. Atmos. Sci.,* **41,** 313–328.
——, and M. J. Nath, 1994: A modeling study of the relative roles of tropical and extratropical SST anomalies in the variability of the global atmosphere–ocean system. *J. Climate,* **7,** 1184–1207.
Lim, G. H., and J. M. Wallace, 1991: Structure and evolution of baroclinic waves as inferred from regression analysis. *J. Atmos. Sci.,* **48,** 1718–1732.
Livezey, R. E., and K. C. Mo, 1987: Tropical–extratropical teleconnections during the Northern Hemispheric winter. Part II: Relationships between monthly mean Northern Hemisphere circulation patterns and proxies for tropical convection. *Mon. Wea. Rev.,* **115,** 3115–3132.
Lorenz, E. N., 1979: Forced and free variations of weather and climate. *J. Atmos. Sci.,* **36,** 1367–1376.
Nakamura, H., 1992: Midwinter suppression of baroclinic wave activity in the Pacific. *J. Atmos. Sci.,* **49,** 1629–1642.
Palmer, T. N., 1993. Extended-range atmospheric prediction and the Lorenz model. *Bull. Amer. Meteor. Soc.,* **74,** 49–66.
——, and D. A. Mansfield, 1986: A study of wintertime circulation anomalies during the past El Niño events using a high resolution general circulation model. II: Variability of the seasonal mean response. *Quart. J. Roy. Meteor. Soc.,* **112,** 639–660.
Peng, P., 1995: Dynamics of stationary wave anomalies associated with ENSO in COLA GCM. Ph.D. dissertation, University of Maryland, College Park, 169 pp. [Available from Dept. of Meteorology, University of Maryland, College Park, MD 20742.]
Quiroz, R. S., 1983: The climate of the "El Nino" winter of 1982–83—A season of extraordinary climatic anomalies. *Mon. Wea. Rev.,* **111,** 1685–1706.
Rasmusson, E. M., and K. Mo, 1993: Linkages between 200-mb tropical and extratropical circulation anomalies during the 1986–1989 ENSO cycle. *J. Climate,* **6,** 595–616.
Reynolds, R. W., 1988: A real-time global sea surface temperature analysis. *J. Climate,* **1,** 75–86.
Sardeshmukh, P. D., and B. J. Hoskins, 1988: The generation of global rotational flow by steady idealized tropical divergence. *J. Atmos. Sci.,* **45,** 1228–1251.
Schonher, T., and S. E. Nicholson, 1989: The relationship between California rainfall and ENSO events. *J. Climate,* **2,** 1258–1269.
Shukla, J., 1984: Predictability of time averages: Part II. The influence of the boundary forcing. *Problems and Prospects in Long and Medium Range Weather Forecasting,* D. M. Burridge and E. Kallen, Eds., Springer-Verlag, 155–206.
——, 1985: Predictability. *Advances in Geophysics,* Vol. 28B, Academic Press, 87–122.
——, and J. M. Wallace, 1983: Numerical simulation of the atmospheric response to equatorial Pacific sea surface temperature anomalies. *J. Atmos. Sci.,* **40,** 1613–1630.
Simmons, A. J., and B. J. Hoskins, 1978: The life cycle of some nonlinear baroclinic waves. *J. Atmos. Sci.,* **35,** 414–432.
——, J. M. Wallace, and G. W. Branstator, 1983: Barotropic wave propagation and instability, and atmospheric teleconnection patterns. *J. Atmos. Sci.,* **40,** 1363–1392.
Smith, I. N., 1995: A GCM simulation of global climate interannual variability: 1950–1988. *J. Climate,* **8,** 709–718.
Snedecor, G. W., and W. G. Cochran, 1978: *Statistical Methods.* 6th ed. Iowa State University Press, 593 pp.
Spencer, R. W., 1993: Global oceanic precipitation from the MSU during 1979–91 and comparisons to other climatologies. *J. Climate,* **6,** 1301–1326.
Stern, W., and K. Miyakoda, 1995: Feasibility of seasonal forecasts inferred from multiple GCM simulations. *J. Climate,* **8,** 1071–1083.
Straus, D. M., 1983: On the role of the seasonal cycle. *J. Atmos. Sci.,* **40,** 303–313.
Ting, M., and I. M. Held, 1990: The stationary wave response to a tropical SST anomaly in an idealized GCM. *J. Atmos. Sci.,* **47,** 2546–2566.
Trenberth, K. E., 1981: Observed Southern Hemisphere eddy statistics at 500 mb: Frequency and spatial dependence. *J. Atmos. Sci.,* **38,** 2585–2605.
——, and J. G. Olson, 1988: ECMWF global analyses 1979–1986: Circulation statistics and data evaluation. NCAR Tech. Note NCAR/TN−300+STR, 94 pp. [Available from the National Center for Atmospheric Research, Boulder, CO 80307.]
——, and J. W. Hurrell, 1994: Decadal atmosphere–ocean variations in the Pacific. *Climate Dyn.,* **9,** 303–319.
van Loon, H., and R. A. Madden, 1981: The Southern Oscillation. Part I: Global associations with pressure and temperature in northern winter. *Mon. Wea. Rev.,* **109,** 1150–1162.
Wallace, J. M., G.-H. Lim, and M. L. Blackmon, 1988: Relationship between cyclone tracks, anticyclone tracks and baroclinic waveguides. *J. Atmos. Sci.,* **45,** 439–462.
Xue, Y., P. J. Sellers, J. L. Kinter III, and J. Shukla, 1991: A simplified biosphere model for global climate studies. *J. Climate,* **4,** 345–364.
Yulaeva, E., and J. M. Wallace, 1994: The signature of ENSO in global temperature and precipitation fields derived from the microwave sounding unit. *J. Climate,* **7,** 1719–1736.